

Microscopic Calculation of Fusion Cross-Sections

Thomas Neff,* Hans Feldmeier, and Karlheinz Langanke

Gesellschaft für Schwerionenforschung mbH, Planckstraße 1, 64291 Darmstadt, Germany

(Dated: October 8, 2018)

A microscopic calculation of cross sections for fusion of oxygen isotopes ^{16}O , ^{22}O and ^{24}O is presented. Fermionic Molecular Dynamics wave functions are used to describe the fully antisymmetrized and angular momentum projected nucleus-nucleus system. The same effective nucleon-nucleon interaction is used to determine the ground state properties of the nuclei as well as the nucleus-nucleus interaction. From the microscopic many-body wave function the corresponding wave function for the relative motion of two point-like nuclei is derived by a method proposed by Friedrich which leads to a local effective nucleus-nucleus potential. Finally the Schrödinger equation with incoming wave boundary conditions is solved to obtain the penetration factors for the different partial waves. With these the S-factor for the fusion process is calculated. A good agreement with experimental data is obtained for the ^{16}O - ^{16}O cross section. Much enhanced cross sections are found for the neutron-rich oxygen isotopes.

PACS numbers: 21.60.-n, 21.60.Gx, 25.60.Pj, 26.50.+x

I. INTRODUCTION

Heavy-ion fusion reactions play important roles in various astrophysical objects. For example, reactions induced by the fusion of two ^{16}O nuclides are the main energy source of hydrostatic oxygen burning [1, 2]. On the other hand pycnonuclear fusion reactions of neutron-rich nuclides are expected to occur in the crust of accreting neutron stars in binary systems, when the ashes of x-ray bursts are pressed to high densities and a series of electron captures has transformed the matter neutron-rich [3, 4]. Electron captures and pycnonuclear fusion generate energies which can affect the dynamics and evolution of the neutron star crust [5].

To determine the relevant fusion cross sections is quite challenging. While for the $^{16}\text{O}+^{16}\text{O}$ reaction data exist at energies below the Coulomb barrier [6, 7, 8, 9], it is yet impossible to determine the cross sections at the most effective energies of hydrostatic oxygen burning ($E \approx 2$ MeV). Hence it has been the standard procedure to extrapolate the measured cross sections down into the energy region of astrophysical interest usually based on phenomenological barrier penetration models [10]. Furthermore, a calculation of the subbarrier $^{16}\text{O}+^{16}\text{O}$ fusion cross sections performed on the basis of the Hartree-Fock model agrees with the data quite well [11]. The situation is significantly more uncertain for the determination of the fusion cross sections for the neutron-rich nuclei. Here no data exist and the cross sections have to be derived solely from theoretical models (e.g. [12]). Furthermore neutron-rich nuclei develop neutron densities with long tails which lead to strongly enhanced fusion probabilities, but are very difficult to systematically describe by parametrized potentials [12].

Obviously it is desirable to base the required extrapo-

lations on theoretical models which are as reliably as possible; i.e. which are accounting for the relevant degrees of freedom of the reaction. In recent years powerful many-body approaches have been developed (Green's Function Monte Carlo [13], No-Core Shell Model [14], Fermionic Molecular Dynamics (FMD) [15, 16, 17]) which allow now a quantitatively correct description of light nuclei based on the solution of the many-body problem for realistic nucleon-nucleon interactions. The next step should be to take advantage of these advances in nuclear structure physics for a more realistic and reliable description of low-energy reaction problems. First attempts have been presented in [18, 19] where microscopic structure information derived from the GFMC or no-core shell model has been incorporated into potential model descriptions of low-energy d+d and p+ ^7Be fusion. Here we will present a different approach, based on the FMD model, which allows for a consistent description of bound, resonant and scattering states from the same many-body Hamiltonian derived from a realistic nucleon-nucleon interaction. In particular, our model describes consistently the internal structure and properties of the asymptotic reaction partners and the relevant degrees of freedom of the collision process. This is particularly important for astrophysically relevant reactions including nuclei far from stability, as their description is usually not constrained by data yet, but it is expected to depend sensitively on nuclear structure subtleties like the formation of neutron halos or skins. While the FMD approach to nuclear reactions is quite general and can be applied to scattering, capture and transfer reactions, we will here present a first application which deals with subbarrier fusion of oxygen isotopes.

We introduce the FMD many-body model in Sec. II. The calculation of the microscopic nucleus-nucleus potential and the transformation into an effective potential for point-like nuclei is performed in the language of the well known Generator Coordinate Method (GCM) and Resonating Group Method (RGM) and is presented in

*Electronic address: t.neff@gsi.de

	^{16}O	^{22}O	^{24}O
E_b / MeV (Experiment)	-127.62	-162.03	-168.48
E_b / MeV (FMD)	-120.07	-153.88	-158.75
r_{matter} / fm (Experiment)	2.54(2)	2.88(6)	3.19(13)
r_{matter} / fm (FMD)	2.50	2.80	2.95

TABLE I: Ground state energies and matter radii calculated with the FMD wave functions. The experimental matter radii are taken from [23].

Sec. III and IV. In Sec. V the fusion cross sections are calculated by solving the Schrödinger equation using incoming wave boundary conditions. In Sec. VI we discuss adiabatic effects before summarizing in Sec. VII.

II. MANY-BODY MODEL

In the Fermionic Molecular Dynamics [15, 16] model the many-body states are described by Slater determinants

$$|\psi\rangle = \mathcal{A}\left\{|q_1\rangle \otimes \dots \otimes |q_A\rangle\right\} \quad (1)$$

using Gaussian wave packets for the single-particle states

$$\langle \vec{x}|q\rangle = \exp\left\{-\frac{(\vec{x}-\vec{b})^2}{2a}\right\} \otimes |\chi^\uparrow, \chi^\downarrow\rangle \otimes |\xi\rangle. \quad (2)$$

The complex parameter \vec{b} encodes the mean position and the mean momentum of the wave-packet. In this paper the width parameter a is chosen to be identical for all single-particle states. The spins can orient freely, the isospin is fixed to describe either a proton or a neutron. The ground state wave function is obtained by minimizing the intrinsic energy with respect to the single-particle parameters a , \vec{b}_i and χ_i . For ^{16}O , ^{22}O and ^{24}O we obtain configurations that are identical to closed-shell harmonic oscillator configurations with a fully occupied $0d_{5/2}$ shell in ^{22}O and a fully occupied $1s_{1/2}$ shell in ^{24}O .

We use a nucleon-nucleon interaction that is derived from the Argonne V18 interaction by explicitly introducing the short-range central and tensor correlations into the many-body system by means of the Unitary Correlation Operator method [20, 21] in a two-body approximation. The correlated interaction has been used successfully in *ab initio* calculations using many-body perturbation theory and the no-core shell model [22]. As the simple FMD wave functions are not able to describe the medium- to long-range tensor correlations we use a phenomenological modification of the two-body interaction as introduced in [16]. Here an additional momentum-dependent two-body part is used and fixed to reproduce the binding energies and radii of ^4He , ^{16}O and ^{40}Ca . An additional spin-orbit term is tuned to the binding-energies of ^{24}O , ^{34}Si and ^{48}Ca .

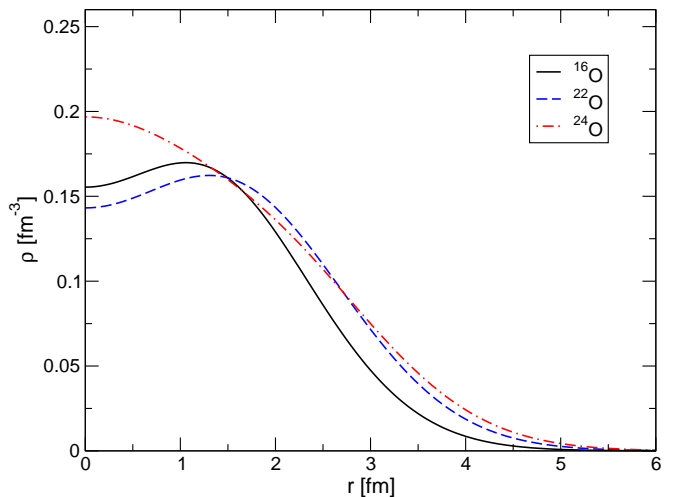


FIG. 1: Matter densities for ^{16}O , ^{22}O and ^{24}O . Finite size of protons and neutrons is taken into account.

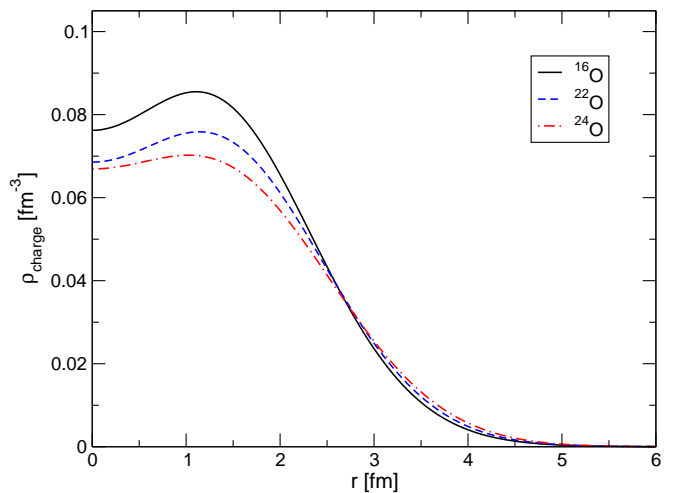


FIG. 2: Charge densities for ^{16}O , ^{22}O and ^{24}O . Finite size of protons and neutrons is taken into account.

The calculated binding energies and matter radii are shown in Tab. I. The ground state densities are shown in Figs. 1, 2. An improved description of the ground states is possible in a variation after projection approach. But as the intrinsic states would then no longer be angular momentum eigenstates, the calculation of the nucleus-nucleus potential would no longer be feasible. As the density distribution remains almost unchanged we expect no significant effect on the nucleus-nucleus potentials and therefore on the fusion cross sections.

III. WAVE FUNCTIONS FOR RELATIVE MOTION

A. GCM wave functions

To calculate the microscopic nucleus-nucleus energy surfaces we make use of the fact that the FMD wave functions can be easily moved and rotated. We construct Generator Coordinate Method (GCM) wave functions using the normalized FMD ground state wave functions $|\psi\rangle$ and the distance $\vec{R} = R\vec{e}_z$ between the origin of the Slater determinants as the generator coordinate. R is assuming values from 0.5 fm up to 15 fm in steps of 0.5 fm

$$|\Psi(\vec{R})\rangle = \mathcal{A} \left\{ |\psi(-\vec{R}/2)\rangle \otimes |\psi(+\vec{R}/2)\rangle \right\}. \quad (3)$$

We have to project these states on angular momentum with the projection operator [24]

$$P_{MK}^J = \frac{2J+1}{8\pi^2} \int d\Omega D_{MK}^{J*}(\Omega) R(\Omega), \quad (4)$$

$\Omega = (\alpha, \beta, \gamma)$ denoting the three Euler angles. As the intrinsic spin of the nuclei is 0^+ the total angular momentum J is given by the orbital angular momentum L of the relative motion of the two nuclei. As the two nuclei are identical we will only encounter even angular momenta and positive parity states. Because of the axial symmetry of the system only the integration over the azimuthal angle β has to be carried out explicitly which we do using a Gauss-Legendre scheme with 50 points. Because of the property

$$(P_{MK}^J)^\dagger P_{M'K'}^{J'} = \delta_{JJ'} \delta_{MM'} P_{KK'}^J, \quad (5)$$

we can calculate the projected GCM Hamiltonian and overlap functions as

$$H^L(R, R') = \frac{4\pi}{2L+1} \langle \Psi(R\vec{e}_z) | (H - T_{\text{cm}}) P_{00}^L | \Psi(R'\vec{e}_z) \rangle \quad (6)$$

and

$$N^L(R, R') = \frac{4\pi}{2L+1} \langle \Psi(R\vec{e}_z) | P_{00}^L | \Psi(R'\vec{e}_z) \rangle. \quad (7)$$

The calculated GCM energy surfaces

$$E^L(R) = \frac{H^L(R, R)}{N^L(R, R)} - (E_{b1} + E_{b2}), \quad (8)$$

where E_{b1} and E_{b2} are the ground state energies of the fragment nuclei, are shown for $L = 0$ in Fig. 3. The GCM energy does not approach the Coulomb potential at large separations as the kinetic energy due to localization of the nuclei is still included. At small separations we can observe the effects of antisymmetrization and saturation that are missing in a double-folding potential.

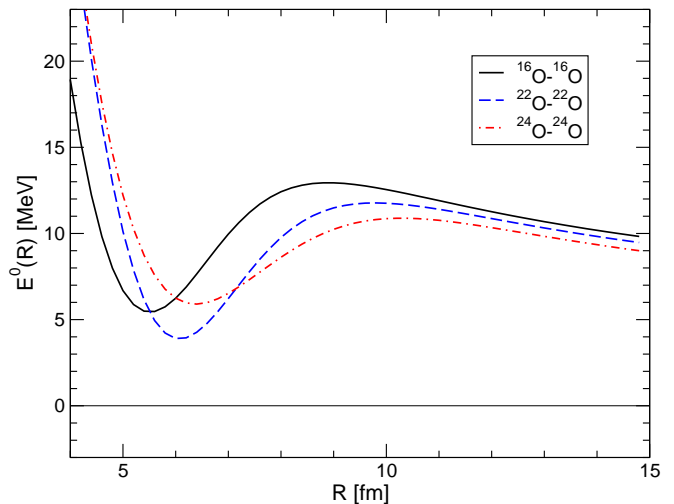


FIG. 3: GCM energy surfaces for $L = 0$. The energy surfaces are different even asymptotically because of different localization energies in the relative motion.

We can fully describe the system of the two nuclei using the GCM basis states Eq. (3)

$$\begin{aligned} |\Psi_{LM}\rangle &= \int dR R^2 P_{M0}^L |\Psi(R\vec{e}_z)\rangle f(R) \\ &\approx \sum_i P_{M0}^L |\Psi(R_i\vec{e}_z)\rangle f_i. \end{aligned} \quad (9)$$

But the GCM “wave function” $f(R)$ can not be interpreted as a wave function for the relative motion of two nuclei. This is because of the non-orthogonality of the basis states. Friedrich [25] proposed a two-step approach for dealing with the non-orthogonality. In a first step a transformation from the GCM into the Resonating Group Method (RGM) basis is performed. This eliminates the non-orthogonality that is caused by the use of Slater determinants in the GCM. In a second step the non-orthogonality due to the antisymmetrization between the two nuclei at short distances is removed.

B. RGM wave functions

In the RGM the wave function for the relative motion of the two nuclei is given using basis states $|\Phi(\vec{r})\rangle$

$$\langle \vec{\rho}, \xi_1, \xi_2 | \Phi(\vec{r}) \rangle = \mathcal{A} \{ \delta(\vec{r} - \vec{\rho}) \phi(\xi_1) \phi(\xi_2) \}. \quad (10)$$

Here $\phi(\xi)$ are the intrinsic wave functions of the nuclei. If all the single-particle states (2) in the GCM Slater determinants have the same width parameter a the GCM basis states can be expressed with the RGM basis states as [26, 27]

$$|\Psi(\vec{R})\rangle = \int d^3r \Gamma(\vec{R} - \vec{r}) |\Phi(\vec{r})\rangle |\Phi_{\text{cm}}\rangle \quad (11)$$

with

$$\Gamma(\vec{R}-\vec{r}) = \left(\frac{\mu}{\pi a}\right)^{3/4} \exp\left(-\mu\frac{(\vec{R}-\vec{r})^2}{2a}\right), \quad \mu = \frac{A_1 A_2}{A_1 + A_2} \quad (12)$$

and the center-of-mass wave function

$$\langle \vec{X} | \Phi_{\text{cm}} \rangle = \left(\frac{A}{\pi a}\right)^{3/4} \exp\left(-A\frac{\vec{X}^2}{2a}\right), \quad A = A_1 + A_2. \quad (13)$$

We introduce the angular momentum projected basis states

$$|\Phi_{LM}(r)\rangle = \sqrt{\frac{4\pi}{2L+1}} P_{M0}^L |\Phi(r\vec{e}_z)\rangle. \quad (14)$$

The RGM norm kernel

$$n_L(r, r') = \langle \Phi_{LM}(r) | \Phi_{LM}(r') \rangle \quad (15)$$

asymptotically behaves as

$$n_L(r, r') \stackrel{r, r' \rightarrow \infty}{\approx} \frac{1 + \delta_{12}(-1)^L}{r^2} \delta(r - r'). \quad (16)$$

In the case of identical nuclei only even L are allowed but an additional factor of two appears in the normalization (exchanging all the nucleons between the two nuclei does not change the wave function).

The angular momentum projected GCM basis state can be expressed by the angular momentum projected RGM basis state as

$$P_{M0}^L |\Psi(R\vec{e}_z)\rangle = \int dr r^2 u_L(R; r) |\Phi_{LM}(r)\rangle |\Phi_{\text{cm}}\rangle \quad (17)$$

with

$$u_L(R; r) = \sqrt{\frac{2L+1}{4\pi}} \Gamma_L(R; r) \quad (18)$$

and

$$\Gamma_L(R; r) = 4\pi \left(\frac{\mu}{\pi a}\right)^{3/4} \exp\left(-\mu\frac{R^2 + r^2}{2a}\right) i_L\left(\mu\frac{Rr}{a}\right), \quad (19)$$

where i_L are the modified spherical Bessel functions [26].

The system of two nuclei (9) can now be described using RGM basis states

$$|\Psi_{LM}\rangle = \int dr r^2 \varphi^{\text{RGM}}(r) |\Phi_{LM}(r)\rangle |\Phi_{\text{cm}}\rangle \quad (20)$$

with the RGM wave function

$$\varphi^{\text{RGM}}(r) = \sum u_L(R_i; r) f_i. \quad (21)$$

C. Collective wave functions

Asymptotically the RGM wave function (21) possesses the properties of a ‘‘proper’’ wave function and can for example be used for implementing boundary conditions. At short distances the RGM norm kernel Eq. (15) deviates from the asymptotic behavior because of the antisymmetrization between the two nuclei. To obtain a wave function that can be identified as a wave function for the relative motion of two point-like nuclei we have to transform the RGM basis states $|\Phi_{LM}(r)\rangle$ into new basis states $|\tilde{\Phi}_{LM}(r)\rangle$ that fulfill

$$\langle \tilde{\Phi}_{LM}(r) | \tilde{\Phi}_{LM}(r') \rangle = \frac{1 + \delta_{12}(-1)^L}{r^2} \delta(r - r'). \quad (22)$$

This is achieved by

$$|\tilde{\Phi}_{LM}(r)\rangle = \int dr' r'^2 |\Phi_{LM}(r')\rangle n_L^{-1/2}(r', r). \quad (23)$$

For the evaluation of the norm kernel we use its spectral representation

$$n_L(r, r') = \sum_{\alpha} \chi^{(\alpha)}(r) \mu^{(\alpha)} \chi^{(\alpha)}(r') \quad (24)$$

where $\mu^{(\alpha)}$ are the eigenvalues and $\chi^{(\alpha)}$ are the (real) eigenvectors of the norm kernel. We perform the diagonalization numerically using the GCM basis states. For that we expand the eigenvectors

$$\chi^{(\alpha)}(r) = \sum_i u_L(R_i; r) \chi_i^{(\alpha)} \quad (25)$$

and transform the integral integration

$$\int dr' r'^2 n_L(r, r') \chi^{(\alpha)}(r') = \mu^{(\alpha)} \chi^{(\alpha)}(r) \quad (26)$$

into the generalized eigenvalue problem

$$\sum_j n_L^{ij} \chi_j^{(\alpha)} = \mu^{(\alpha)} \sum_j \eta_L^{ij} \chi_j^{(\alpha)} \quad (27)$$

with

$$\begin{aligned} n_L^{ij} &= \int dr r^2 \int dr' r'^2 u_L(R_i; r) n_L(r, r') u_L(R_j; r') \\ &= \langle \Psi(R_i \vec{e}_z) | P_{00}^L | \Psi(R_j \vec{e}_z) \rangle \end{aligned} \quad (28)$$

and

$$\eta_L^{ij} = \int dr r^2 u_L(R_i; r) u_L(R_j; r). \quad (29)$$

We can now express the GCM basis state as

$$P_{M0}^L |\Psi(R_i \vec{e}_z)\rangle = \int dr r^2 \tilde{u}_L(R_i; r) |\tilde{\Phi}_{LM}(r)\rangle |\Phi_{\text{cm}}\rangle \quad (30)$$

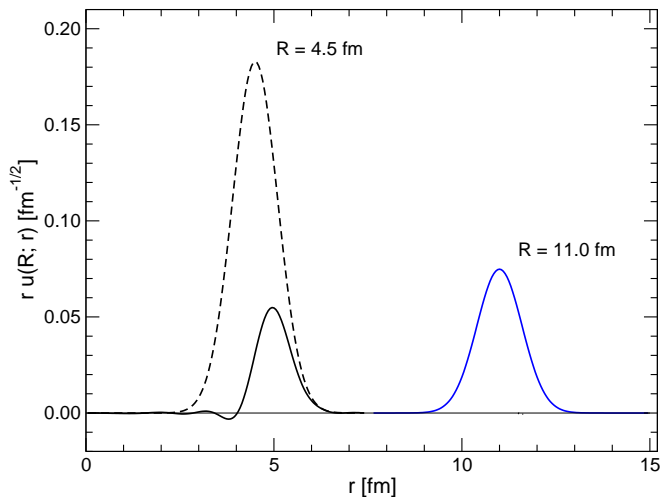


FIG. 4: The wave functions $ru_L(R; r)$ (dashed lines) and $r\tilde{u}_L(R; r)$ (solid lines) for $^{16}\text{O}-^{16}\text{O}$, $L = 0$ at $R = 4.5$ fm and $R = 11$ fm. $\tilde{u}_L(R, r)$ is suppressed at small distances due to antisymmetrization.

with

$$\begin{aligned} \tilde{u}_L(R_i; r) &= \int dr' r'^2 n_L^{1/2}(r, r') u_L(R_i; r') \\ &= \sum_k u_L(R_k; r) \sum_l \left(\sum_\alpha \chi_k^{(\alpha)} \sqrt{\mu^{(\alpha)}} \chi_l^{(\alpha)} \right) \eta_L^{li}. \end{aligned} \quad (31)$$

The effects of antisymmetrization are illustrated in Fig. 4 where $u_L(R; r)$ and $\tilde{u}_L(R; r)$ are shown for small and large separations. At large separations u_L and \tilde{u}_L coincide while at $R = 4.5$ fm, where there is a large overlap between the surfaces of the nuclei, \tilde{u} is substantially reduced and shifted outwards due to antisymmetrization. Completely Pauli forbidden states correspond to eigenvalues $\mu = 0$. For large separations the antisymmetrization between the clusters has no effect and the eigenvalues μ approach 1.

For a state described in the GCM world as

$$|\Psi_{LM}\rangle = \sum_i P_{M0}^L |\Psi(R_i \vec{e}_z)\rangle f_i \quad (32)$$

the corresponding proper wave function for the relative motion is given by

$$\varphi_L(r) = \sum_i \tilde{u}_L(R_i; r) f_i. \quad (33)$$

IV. NUCLEUS-NUCLEUS POTENTIALS

In principle the transformation procedure defines an energy independent effective interaction but it has a complicated non-local structure. We will therefore follow

Friedrich [25] and fit a local potential to the GCM matrix elements.

When comparing the GCM overlap matrix elements with the corresponding expression in the collective world

$$\langle \Psi(R_i \vec{e}_z) | P_{00}^L | \Psi(R_i \vec{e}_z) \rangle \stackrel{!}{=} \int dr r^2 \tilde{u}_L(R_i; r) \tilde{u}_L(R_i; r) \quad (34)$$

we observe numerical deviations for $R_i \leq 3.5$ fm where $\tilde{u}_L(R_i; r)$ is almost completely suppressed. As we will solve the Schrödinger equation with incoming wave boundary conditions, we will need the solution of the Schrödinger equation only from the minimum in the potential surface outwards to calculate the barrier penetration. We therefore fit the Hamiltonian matrix elements only for $R_i \geq 4.0$ fm. Our ansatz for the effective Hamiltonian in the collective world is given by

$$H_{\text{eff}}^L(r) = \frac{p_{\text{rel}}^2}{2\mu M_N} + \frac{L(L+1)}{2\mu M_N r^2} + V_{\text{eff}}^L(r) + V_C(r) + E_{b1} + E_{b2} \quad (35)$$

where the Coulomb interaction is that of two homogeneously charged spheres (r_c is taken to be the charge radius)

$$V_C(r) = \begin{cases} Z_1 Z_2 e^2 \frac{1}{r} & ; r > 2r_c \\ Z_1 Z_2 e^2 \left(3 - \frac{r^2}{r_c^2}\right) \frac{1}{2r_c} & ; r < 2r_c \end{cases} \quad (36)$$

The effective potential $V_{\text{eff}}^L(r)$ is parameterized as a sum of ten Gaussians. We minimize the deviation from the GCM matrix elements to fulfill the relation

$$\begin{aligned} \langle \Psi(R_i \vec{e}_z) | (H - T_{\text{cm}}) P_{00}^L | \Psi(R_i \vec{e}_z) \rangle \stackrel{!}{=} \\ \int dr r^2 \tilde{u}_L(R_i; r) H_{\text{eff}}^L(r) \tilde{u}_L(R_i; r) \end{aligned} \quad (37)$$

as well as possible. We determine $V_{\text{eff}}^L(r)$ independently for $L = 0, 2, 4$ and obtain almost identical fits. Therefore a L -independent $V_{\text{eff}}(r)$ is chosen and fitted simultaneously to the $L = 0, 2, 4$ matrix elements. The deviations between the collective and GCM matrix elements are less than 50 keV.

The fitted $L = 0$ effective potentials including the Coulomb interaction are shown in Fig. 5. As could already be deduced from the GCM energy surfaces the neutron rich isotopes feature lowered barriers at larger distances due to the attractive nuclear interaction in the tails of the neutron distribution.

V. FUSION CROSS SECTIONS

With the effective potential derived in the last section the two-body Schrödinger equation

$$\left[\frac{p_{\text{rel}}^2}{2\mu M_N} + \frac{L(L+1)}{2\mu M_N r^2} + V_{\text{eff}}(r) + V_C(r) \right] \varphi_L(r) = E \varphi_L(r) \quad (38)$$

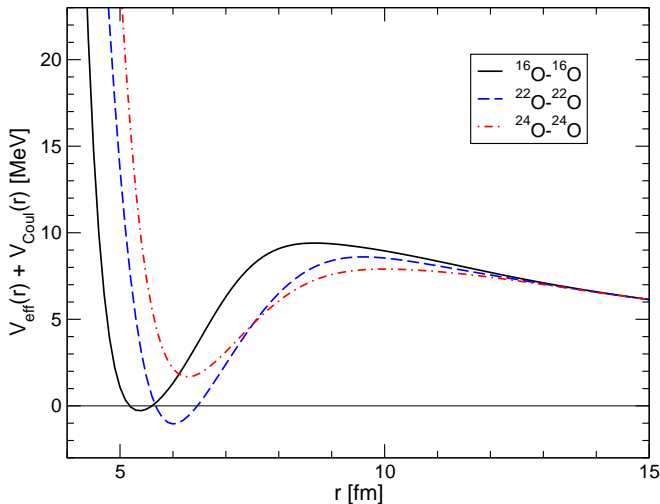


FIG. 5: Effective Nucleus-Nucleus Potentials ($L = 0$) derived from the FMD energy surfaces. The barrier gets lower and shallower with increased neutron number.

is solved with Incoming Wave Boundary Conditions (IWBC) [28]. No imaginary part of the potential is needed in this approach. We assume that the nuclei will fuse when the minimum in the potential surface has been reached. The IWBC can be formulated as

$$\frac{\varphi'_L(r_{\min})}{\varphi_L(r_{\min})} = ik_L(r_{\min}) \quad (39)$$

where $k_L(r)$ is the local wave number

$$k_L(r) = \sqrt{2\mu M_N \left(E - \frac{L(L+1)}{2\mu M_N r^2} - V_{\text{eff}}(r) - V_C(r) \right)}. \quad (40)$$

The Schrödinger equation is integrated numerically starting from r_{\min} outwards and matched to the Coulomb scattering solution

$$\varphi_L^{\text{Coul}}(r) = C_- (F_L(kr) - iG_L(kr)) + C_+ (F_L(kr) + iG_L(kr)) \quad (41)$$

with

$$k = \sqrt{2\mu M_N E}. \quad (42)$$

The matching point r_m has to be outside the range of the nuclear potential $V_{\text{eff}}(r)$. The penetration factor P_L is given by the ratio of the incoming flux at r_{\min} to the incoming Coulomb flux

$$P_L = \frac{k_L(r_{\min})}{k|C_-|^2}. \quad (43)$$

For very low energies ($E < 4$ MeV) the magnitude of the transmission coefficient gets very small and the numerical matching is no longer possible. For these energies we use the approximation [29]

$$P_L \approx \frac{k_L(r_{\min})}{k_L(r_m)} \frac{|\varphi_L(r_{\min})|^2}{|\varphi_L(r_m)|^2} \frac{4F_L^2(kr_m)}{F_L^2(kr_m) + G_L^2(kr_m)}. \quad (44)$$

With the penetration factors we immediately obtain the fusion cross section

$$\sigma(E) = \frac{\pi}{k^2} \sum_{L=0}^{L_{\text{crit}}} (1 + \delta_{12}(-1)^L) (2L+1) P_L(E). \quad (45)$$

As we are dealing with the fusion of identical nuclei only even angular momenta L contribute to the cross section.

Instead of the cross section we plot in Fig. 6 the astrophysical S-factor where the tunneling through a point-charge s -wave Coulomb barrier has been taken out of the cross section

$$S(E) = \sigma(E) E e^{2\pi\eta}. \quad (46)$$

For ^{16}O the agreement with the available data is satisfactory, taking the fact into account that no parameters have been adjusted. The observed edge in the S-factor is related to the barrier height (see Fig. 5). In the case of ^{24}O no fusion occurs below $E_{\text{cm}} = 2$ MeV because the potential calculated with frozen configurations does not drop below zero inside the Coulomb barrier. In the following section we will discuss the adiabatic energy surface for which the S-factor will smoothly continue to $E_{\text{cm}} = 0$.

Comparing the neutron rich oxygen isotopes with ^{16}O we find fusion cross sections that are enhanced by 6-8 orders of magnitude. This is caused by the reduction of the height and width of the Coulomb barriers for the neutron rich ^{22}O and ^{24}O .

In the last years a hindrance of the fusion process at sub-barrier energies compared to coupled channel calculations has been found for medium-heavy nuclei ([30] and references therein). In [31] this effect was related to a shallower potential due to the saturation properties of nuclear matter that become important for large overlap of the reacting nuclei. In a recent paper [32] a drop-off of the S-factor in the ^{16}O - ^{16}O fusion reaction has been predicted for energies below 7 MeV due to this fusion hindrance effect. Although our wave functions are fully antisymmetrized products of frozen ground states and therefore saturation effects are included explicitly we do not find such a decrease in the S-factor. The nucleus-nucleus potential while featuring only a shallow minimum still allows for an increase in the S-factor for energies well below the barrier.

VI. ADIABATIC EFFECTS

Up to now we have discussed the fusion process in a single-channel approximation where the nuclei stay in their ground states. To describe effects beyond the single-channel approximation we could in principle extend our discussion to a coupled-channel approach by including excited states and trying to derive the coupling potentials.

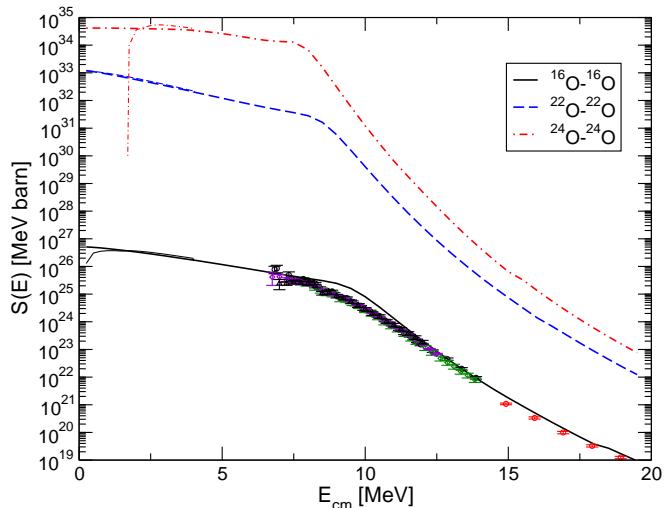


FIG. 6: S-factor for the fusion of oxygen isotopes. Experimental data [6, 7, 8, 9] for ^{16}O are included. The S-factor is calculated with the effective potential derived for the frozen configurations (thin lines) and with the modified potentials for the adiabatic configurations (thick lines).

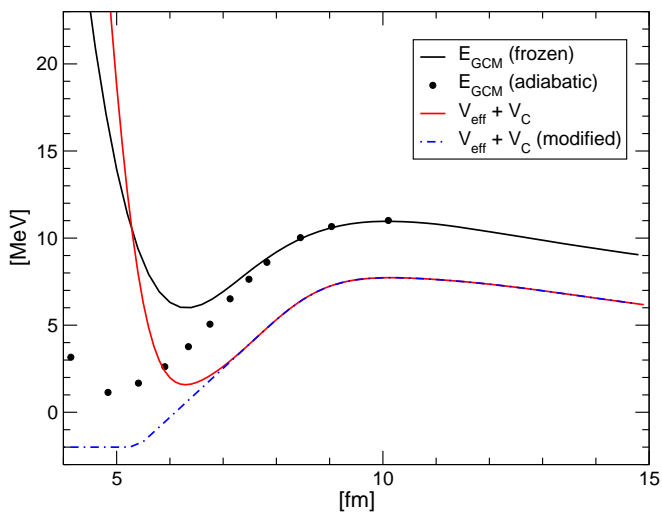


FIG. 7: GCM energy surfaces for the ^{24}O - ^{24}O system calculated with frozen configurations (solid line) and with FMD configurations minimized under quadrupole constraints (dots). The intrinsic quadrupole deformation is mapped on the separation R between the nuclei. The effective nucleus-nucleus potential derived from the frozen GCM configs is given by the dashed line.

Another point of view is to switch from the diabatic picture with frozen configurations to an adiabatic approach where we allow for distortions of the wave functions. We generate such wave functions by minimizing the expectation value of the energy for the $2A$ -nucleon system with respect to the parameters of all the FMD

single particle states under constraints on the quadrupole deformation of the total intrinsic wave function. For these configurations we define the separation distance to be that of the frozen configuration with the same quadrupole deformation. The adiabatic GCM energy surface calculated for ^{24}O can be seen in Fig. 7. We see almost no effect in the region of the Coulomb barrier but observe less repulsion at smaller separations. The corresponding adiabatic wave functions can no longer be expressed with RGM wave functions and therefore the derivation of the effective nucleus-nucleus potential as done for the frozen configurations is not possible any more. To estimate the effects of the adiabatic configurations we modify the nucleus-nucleus potential as shown in Fig. 7 to reflect the changes seen in the GCM energy surface. These modifications change the low energy behavior especially in the ^{24}O - ^{24}O case where the nucleus-nucleus potential for the frozen configurations has a minimum above zero energy. The modified potential goes below zero and the S-factor now smoothly continues to $E_{\text{cm}} = 0$. A similar but less pronounced effect can be seen for ^{16}O - ^{16}O , whereas the ^{22}O - ^{22}O S-factor stays almost unchanged. Variations of the depth of the modified potential from -0.5MeV to -10MeV change the S-factor by less than 50%.

VII. SUMMARY AND CONCLUSION

In this paper we studied the fusion cross sections for the oxygen isotopes ^{16}O , ^{22}O and ^{24}O in the Fermionic Molecular Dynamics model. The same effective nucleon-nucleon interaction is used for the ground states and the two-nucleus system. The total wave function is antisymmetrized and projected on angular momentum eigenstates. In a two-step process an effective nucleus-nucleus potential is derived from the GCM energy surface. The Schrödinger equation is solved with incoming wave boundary conditions to obtain the fusion cross sections. Effects beyond the frozen ground state approximation are studied with adiabatic configurations obtained as FMD many-body states under constraints on the quadrupole deformation. Experimental data on ^{16}O - ^{16}O are reproduced; a much enhanced cross section for the fusion of the neutron-rich oxygen isotopes is found.

Acknowledgments

We are grateful to Michael Wiescher for suggesting to investigate fusion cross sections in the FMD approach and thank him and Leandro Gasques for fruitful discussions. T.N. acknowledges the support by The Joint Institute for Nuclear Astrophysics (JINA) NSF PHY 0216783.

-
- [1] C. E. Rolfs and W. S. Rodney, *Cauldrons in the Cosmos* (Chicago Press, 1988).
- [2] S. E. Woosley, A. Heger, and T. A. Weaver, *Rev. Mod. Phys.* **74**, 1015 (2002).
- [3] P. Haensel and J. L. Zudnik, *Astron. Astrophys.* **227**, 431 (1990).
- [4] P. Haensel and J. L. Zudnik, *Astron. Astrophys.* **404**, 33 (2003).
- [5] L. Bildsten, *Astrophys. J.* **501**, 89 (1998).
- [6] H. Spinka and A. Winkler, *Astrophys. J.* **174**, 455 (1972).
- [7] G. Hulke, C. Rolfs, and H. P. Trautvetter, *Z. Phys.* **A297**, 161 (1980).
- [8] S. C. Wu and C. A. Barnes, *Nucl. Phys.* **A422**, 373 (1984).
- [9] J. Thomas, Y. T. Chen, S. Hinds, D. Meredith, and M. Olson, *Phys. Rev. C* **33**, 1679 (1986).
- [10] G. R. Caughlan, W. A. Fowler, and B. A. Zimmermann, *At. Data Nucl. Data Tables* **40**, 283 (1988).
- [11] P.-G. Reinhard, J. Friedrich, K. Goeke, F. Grümmer, and D. H. E. Gross, *Phys. Rev. C* **30**, 878 (1984).
- [12] L. R. Gasques, L. C. Chamon, D. Pereira, M. A. G. Alvarez, E. S. Rossi, C. P. Silva, and B. V. Carlson, *Phys. Rev. C* **69**, 034603 (2004).
- [13] R. B. Wiringa, S. C. Pieper, J. Carlson, and V. R. Pandharipande, *Phys. Rev. C* **62**, 014001 (2000).
- [14] P. Navratil and B. R. Barrett, *Phys. Rev. C* **57**, 3119 (1998).
- [15] H. Feldmeier and J. Schnack, *Rev. Mod. Phys.* **72**, 655 (2000).
- [16] R. Roth, T. Neff, H. Hergert, and H. Feldmeier, *Nucl. Phys.* **A745**, 3 (2004).
- [17] M. Chernykh, H. Feldmeier, T. Neff, P. von Neumann-Cosel, and A. Richter, *Phys. Rev. Lett* **98**, 032501 (2007).
- [18] A. Arriaga, V. R. Pandharipande, and R. Schiavilla, *Phys. Rev. C* **43**, 983 (1991).
- [19] P. Navratil, C. A. Bertulani, and E. Caurier, *Phys. Rev. C* **73**, 065801 (2006).
- [20] T. Neff and H. Feldmeier, *Nucl. Phys.* **A713** (2003).
- [21] R. Roth, H. Hergert, P. Papakonstantinou, T. Neff, and H. Feldmeier, *Phys. Rev. C* **72**, 034002 (2005).
- [22] R. Roth, P. Papakonstantinou, N. Paar, H. Hergert, T. Neff, and H. Feldmeier, *Phys. Rev. C* **73**, 044312 (2006).
- [23] A. Ozawa, T. Suzuki, and I. Tanihata, *Nuc. Phys.* **A693**, 32 (2001).
- [24] P. Ring and P. Schuck, *The Nuclear Many-Body Problem* (Springer, 2000).
- [25] H. Friedrich, *Phys. Rept.* **74**, 209 (1981).
- [26] H. Horiuchi, in *Cluster models and other topics*, edited by H. Horiuchi and K. Ikeda (World Scientific Publishing, 1986).
- [27] D. Baye, P.-H. Heenen, and M. Libert-Heinemann, *Nuc. Phys.* **A291**, 230 (1977).
- [28] G. H. Rawitscher, *Nuc. Phys.* **85**, 337 (1966).
- [29] P. R. Christensen and Z. E. Switkowski, *Nuc. Phys.* **A280**, 205 (1977).
- [30] C. L. Jiang, B. B. Back, H. Esbensen, R. V. F. Janssens, and K. E. Rehm, *Phys. Rev. C* **73**, 014613 (2006).
- [31] S. Misiu and H. Esbensen, *Phys. Rev. Lett.* **96**, 112701 (2006).
- [32] C. L. Jiang, K. E. Rehm, B. B. Back, and R. V. F. Janssens, *Phys. Rev. C* **75**, 015803 (2007).